NASA TM-86257

NASA Technical Memorandum 86257

NASA-TM-86257 19840021814

DESIGN OF A CANDIDATE FLUTTER SUPPRESSION CONTROL LAW FOR DAST ARW-2

William M. Adams, Jr. and

Sherwood H. Tiffany

July 1984

NASA

National Aeronautics and
Space Administration

Langley Research Center
Hampton, Virginia 23665

DESIGN OF A CANDIDATE FLUTTER SUPPRESSION CONTROL LAW FOR DAST ARW-2

William M. Adams, Jr. and Sherwood H. Tiffany
NASA Langley Research Center
Hampton, Virginia

ABSTRACT

A control law is developed to suppress symmetric flutter for a mathematical model of an aeroelastic research vehicle. An implementable control law is attained by including modified LQG (Linear Quadratic Gaussian) design techniques, controller order reduction, and gain scheduling. An alternate (complementary) design approach is illustrated for one flight condition wherein nongradient-based constrained optimization techniques are applied to maximize controller robustness.

NOMENCLATURE

a_i, a_i'	i^{th} element of vector of design variables used in design of robust reduced order controller and its related transformation (see Eq. (21))
a_{u_i}, a_{ℓ_i}	upper and lower bound on ith design variable
$(a_w')^*$	value of a' vector which maximizes minimum singular value for a specific weighting matrix
(A,B_u,B_w)	state, control and noise distribution matrices in plant state equation
(A_c,B_c)	controller state and input distribution matrices
$A_0,A_1,\ldots,A_{n_\ell+2}$	real coefficient matrices in unsteady aerodynamic force approximation
b	reference length
b_ℓ	ℓth constant in denominator of expression for $\hat{Q}$ (See Eq. (4))
c	vector of inequality constraints entering into constrained optimization

N84-29883#

c_u, c_ℓ	upper and lower limits on constraint variable vector
$\bar{c}$	vector of inequality constraint violations
(C, D_u, D_w)	state, control and noise distribution matrices in plant output equations
D	matrix of viscous damping force coefficients
F	regulator gain
$\tilde{F}$	reduced order controller gain magnitude, degrees/g
$\tilde{F}_o$	gain magnitude of initial, unscheduled, reduced order controller, degrees/g
F_m	gain margin
G	plant transfer function (y/u_R), FS-off
g	acceleration due to gravity
h	altitude
H	controller transfer function (u_{FS}/y)
J_R, J_E	regulator and estimator performance indices
K	generalized stiffness matrix
k	reduced frequency
L	Kalman estimator gain
M	generalized mass matrix
$\bar{M}$	Mach number
N_c	number of counterclockwise encirclements of the −1 point by the open loop transfer function as ω varies from 0 to ∞
$n_\xi, n_\delta, n_g, n_o, n_\ell$	number of generalized coordinates, controls, gusts, outputs, and unsteady aerodynamic lag coefficients
P	steady-state convariance of state estimate
$Q, \hat{Q}$	matrix of generalized aerodynamic force coefficients and its s-plane approximation, respectively.
q	dynamic pressure
R_u, R_g, R_m	intensities of control, gust and measurement noises
R_1, R_2	state and control weighting matrices in regulator design
S	closed loop, steady-state covariance matrix
s	Laplace variable
T(s)	fixed portion of reduced order controller
t	time
U	airspeed
u	commanded control input
u_{FS}	negative of commanded control input from FS control law
u_r	reference input command

V	$V = \begin{bmatrix} V_1 & V_{12} \\ V_{12}^T & V_2 \end{bmatrix}$ is process and measurement noise intensity matrix
W	diagonal weighting matrix in augmented performance function (see Eq. (22))
W_g	gust velocity
w	$w^T=(w_u^T, w_g^T, w_m^T)$ is a vector of zero mean, white noise errors in the input, white noise driving the gust filter and white noise in the measurements, respectively
x	$x^T=(\xi^T, \dot{\xi}^T, x_{\ell_1}^T, \ldots, x_{\ell_{n_\ell}}^T, x_A^T, x_g^T)$ is plant state vector
$\hat{x}$	plant state vector estimate
δ	vector of control rotations
δ_a, δ_{a_c}	outboard aileron and commanded outboard aileron rotations, respectively
ξ	vector of generalized coordinates
σ_{min}	minimum singular value
ϕ_m	phase margin
Φ_W	augmented performance function minimized in constrained optimization solution for robust controller (see Eq. (22))
ω	frequency, rad/sec
$(\tilde{\ })$	reduced order
$E()$	expected value

INTRODUCTION

This paper describes the design of a control law for suppression of symmetric flutter for a mathematical model of the DAST (Drones for Aerodynamic and Structural Testing) ARW-2 (Aeroelastic Research Wing Number 2) aircraft. An implementable control law is attained by including the following elements in the design process: development of linear, time-invariant state space evaluation and design models that include unsteady aerodynamic force effects (Refs. 1-4); use of LQG (Linear Quadratic Gaussian) methods for full order controller design including robustness recovery (Refs. 5,6); definition of a candidate reduced order controller (Refs. 7-9); and development of a gain schedule to improve off design performance.

Results are presented which indicate how the evaluation and design models of the plant are defined. The control problem is exhibited by displaying the flutter characteristics of the uncontrolled vehicle and by stipulating the design criteria. A description is given of the methodology employed in determining the full and reduced order controllers; and the performance of the scheduled reduced order controller is shown both at the design point and at off design conditions.

The DAST ARW-2 will employ what is effectively a single-input/single-output control law for suppression of flutter in the symmetric degrees of freedom. Consequently, robustness can be characterized in terms of gain margins, phase margins, minimum eigenvalue (singular value) of the return difference transfer function and high frequency characteristics of the controller. Robustness constraints were not explicitly included in the design algorithm used to define the scheduled reduced order controller. Instead, robustness characteristics were examined offline and improved by repeating the design using the robustness recovery procedure (Ref. 6).

One example is also shown where constrained optimization techniques (Refs. 10-13) are utilized to explicitly include robustness criteria within the design algorithm. The minimum singular value of the return difference matrix is maximized subject to constraints on stability, control power, gain margins, and phase margins. A similar approach, which employs a gradient-based optimizer, has been applied to improve the robustness of a lateral stability augmentation control law (Ref. 14). The nonlinear programming algorithm (Refs. 15,16), selected here to perform the optimization, requires no gradient computation and has recently been successfully applied to several design problems (Refs. 13,17,18).

DAST ARW-2 SUMMARY

The primary objective of the DAST ARW-2 research is to provide a partial assessment of the validity of applying current analysis and design techniques in the design of actively controlled aircraft. In this activity a remotely piloted drone which will incorporate several active control functions has been designed and built and will be flight tested. Correlation of experimentally measured and analytically predicted performance will be documented.

The ARW-2 wing has a supercritical airfoil, a 10.3 aspect ratio and a 25° sweep at the quarter chord. It was purposely designed to require flutter suppression (FS), maneuver load alleviations (MLA) and gust load alleviation (GLA) in some flight regimes. Furthermore, the wing was positioned on the fuselage so as to require relaxed static stability (RSS) augmentation to achieve satisfactory handling characteristics.

An early phase of research (Refs. 19,20) defined actuator requirements, identified desirable sensor locations and developed preliminary active control laws. Refinement of the modeling and control law design has resulted in the analog implementation of the control laws into hardware. This hardware has been constructed such that gain and filter constants can be changed and new compensation can be added, if necessary, as the knowledge of the aircraft becomes more precise. The undocumented structural model employed in this paper is the same as that used in obtaining the currently implemented control laws. It is similar to that of references 19 and 20.

The wings have been constructed at NASA Langley, the control hardware and actuators have been installed, and ground vibration and static loads tests with the wing cantilevered have been conducted. A more detailed structural model is under development which is being tempered by the experimental data. When the updated structural model is completed, the FS design will be repeated for the symmetric case and an antisymmetric FS law will be developed.

Figure 1 depicts the sensors and control surface that will be employed in the symmetric FS control law and defines how the sensor signals are separated into symmetric components prior to compensation.

MATHEMATICAL MODELS

Evaluation Model

Modal Characteristics.- A modal characterization of the aircraft is employed which resulted from performing a free-free vibration analysis of the ARW-2. Twelve modes are retained for the symmetric degrees of freedom which are mean-body vertical displacement and pitch and ten symmetric elastic modes. Table 1 lists the natural, in vacuum, frequencies associated with each of the elastic modes and figure 2 shows the normal components of the first six symmetric elastic mode shapes. Fore and aft motion, not shown in the plots, predominates for elastic mode 3.

Unsteady Aerodynamics Force Computation.- Unsteady aerodynamic force coefficients are computed using a doublet lattice (Refs. 21,22) module contained in the ISAC (Interaction of Structures, Aerodynamics and Controls) program (Ref. 1). The paneling of the lifting surfaces that was employed is shown in figure 3. The circles shown indicate points at which modeshape data are defined. Aerodynamic force coefficients are computed for a number of Mach numbers and, at each Mach number, for the following set of reduced frequencies.

(0.0, 0.005, 0.01, 0.05, 0.1, 0.2, 0.3, 0.4, 0.5, 0.6, 0.8, 1.0)

Reduced frequency satisfies the following relationship

$$k = \frac{\omega b}{U} \qquad (1)$$

where b is a reference length (chosen here to be one half the mean aerodynamic chord of the wing), U is airspeed and ω is frequency of oscillation in rad/sec.

Frequency Domain Equations.- Given the modal characteristics and associated aerodynamic force coefficients, a frequency domain form of the equations of motion can be written.

$$\left[-M\omega^2+Di\omega+K+qQ_\xi\right]\{\xi\} + \left[-M_\delta\omega^2+qQ_\delta \vdots \frac{q}{U} Q_g\right]\left\{\begin{matrix}\delta \\ W_g\end{matrix}\right\} = \{0\} \qquad (2)$$

where

$\{\xi\}$	is a vector of generalized coordinates
$\{\delta\}$	is a vector of control rotations
$\{W_g\}$	is a vector of gust velocity components
M,D,K	are generalized masses, dampings and stiffnesses, respectively (damping ratios of 0.005 were assumed for each elastic mode)
M_δ	is control mass coupling matrix

$Q(k,\overline{M})=[Q_\xi:Q_\delta:Q_g]$ is a matrix of unsteady aerodynamic force coefficients which is complex and frequency and Mach number dependent

and

q is dynamic pressure

In this form of the equations of motion, the assumption is made that control surface actuators are sufficiently powerful that aerodynamic hinge moments and inertial cross coupling hinge moments do not affect control position (rotation).

The following transfer function representation of the actuator with aileron attached is employed in both the evaluation model and the design model to relate control deflection to commanded control deflection:

$$\delta_a = \frac{180}{s+180} \; \frac{314^2}{s^2+251s+314^2} \; \delta_{a_c} \tag{3}$$

This representation fits the experimentally determined frequency response up to 300 rad/sec.

S-plane Aerodynamic Force Approximation.- An approximation to the unsteady aerodynamic force coefficients is made in order to convert equation (2) into a set of first order, time-invariant state equations more amenable to linear systems analysis and design techniques. A least squares curve fit is made, for a specific Mach number, of the matrix of frequency dependent coefficients using a matrix function of the form (Refs. 3,23-26).

$$\hat{Q}(k) = A_0 + A_1 ik + A_2(ik)^2 + \sum_{\ell=1}^{n_\ell} \frac{ikA_{\ell+2}}{(b_\ell+ik)} \,. \tag{4}$$

In the evaluation model, n_ℓ is 4 and the b_ℓ are 0.0939, 0.1878, 0.2817, 0.3756. Linear constraints are imposed upon the rigid body columns of the A_i matrices which require that the curve fit match the tabular data and its slope at $k = 0$ (Ref. 27). In addition, the A_2 column corresponding to the gust mode is constrained to be zero.

State Space Equations of Motion.- Under the assumption that the curve fit in equation (4) for $s = i\,U/b\,k$ is valid for points off the imaginary axis, linear, time-invariant equations of motion can be written of the form

$$\dot{x} = Ax + B_u u + B_w w$$

with outputs

$$y = Cx + D_u u + D_w w \tag{5}$$

where

$$x^T = (\xi^T, \dot{\xi}^T, x_{\ell_1}^T, \ldots, x_{\ell_{n_\ell}}^T, x_A^T, x_g^T)$$

$x_{\ell_1}, \ldots, x_{\ell_{n_\ell}}$ are $n_\ell x n_\xi$ states associated with the unsteady aerodynamic force representation (Refs. 2,3)

x_A are states representing actuator transfer functions

x_g are gust states--the Dryden spectrum is assumed (Ref. 28)

u are commanded control inputs

w $w^T = (w_u^T, w_g^T, w_m^T)$ are uncorrelated zero mean, white noise processes with intensities R_u, R_g, R_m, respectively

B_w $B_w = [B_u : B_g : 0]$

D_w $D_w = [D_u : D_g : I]$

The evaluation model plant state vector is 77 by 1.

Design Model

A reduced order model of the plant was developed in order to lower the cost of the design of the control law. Only two lag terms were retained in the s-plane approximation of the unsteady aerodynamic forces, equation (4). The values selected for the denominator coefficients, ($b_1 = 0.31, b_2 = 0.71$) yield a good fit to the computed aerodynamic data.

A subset of the modes in equation (2) was selected for retention. Modes with natural frequencies below or near the open loop flutter frequency (116 rad/sec for $\overline{M} = 0.86$) which were observed to have little effect upon the flutter characteristics were truncated. Vertical translation pitch, and the second elastic mode, (see Fig. 2), were truncated. Modal residualization (Refs. 4,8,13,29) was employed to retain the static effects of the four highest frequency modes. Thus, five modes were retained in the design model. The resulting state space representation of the design model of the plant has 25 state variables (10 vehicle, 10 aerodynamic, 3 actuator, 2 gust).

Figure 4 is a Bode plot comparison of the amplitude of the symmetric signal to be sent to the controller per unit commanded control input for the design and evaluation models. This figure shows that the reduced order design model is in good agreement with the full order evaluation model (phase angle comparisons, not shown, also exhibit excellent agreement at frequencies below 500 rad/sec).

DESIGN OF CONTROL LAWS

Design Criteria

Flutter Boundaries.– Figure 5 shows three boundaries. The predicted flutter boundary (FS-off) is shown as the solid line. Flutter occurs, for the uncontrolled aircraft, to the right of this line. The dashed line, which will be referred to as the nominal stability margin boundary, is a boundary to the left of which the FS control law should provide stability with ±6dB gain margins and ±45° phase margins. The third curve, denoted as the desired closed loop flutter boundary, defines a boundary to the left of which the FS control should provide stability with no constraints on stability margins.

Control Law Design and Evaluation Points.– The control law design point in this study is at an altitude of 15,000 feet and a Mach number of 0.86. This point is indicated on figure 5. Off design performance of the control law is evaluated at selected points which are also shown on figure 5.

Control Constraints.– The peak deflection and rate capabilities for the outboard ailerons are ±15° and ±740°/sec, respectively. The control law is to be designed such that saturation does not occur, in the root mean square (rms) sense, for an input gust spectrum having an rms of 12 feet/sec. The control saturation constraints are to be satisfied at all points to the left of the nominal stability margin boundary of figure 5. The Dryden spectrum is assumed for the design phase and the von Karman spectrum is used for controller evaluation.

Altitude Root Loci.– Figure 6 shows the characteristic roots as a function of altitude (FS-off, $\overline{M}$ = 0.86) for the symmetric evaluation model. Flutter is predicted to occur at 18,750 feet (q = 531 lb/ft^2). The design point dynamic pressure is 16.5 percent higher than the dynamic pressure at the flutter point.

Full Order Controller Design

The ISAC (Ref. 1) program was used to generate the reduced order design model of the plant. The resulting linear, time-invariant equations are

$$\begin{aligned} \dot{\tilde{x}} &= \tilde{A}\tilde{x} + \tilde{B}_u u + \tilde{B}_w w \\ \tilde{y} &= \tilde{C}\tilde{x} + \tilde{D}_w w \end{aligned} \tag{6}$$

where $(\tilde{A},\tilde{B}_u)$ is stabilizible and $(\tilde{A}^T,\tilde{C}^T)$ is reconstructible.

LQG algorithms in the ORACLS (Ref. 5) program were then employed to obtain full order controllers, with respect to the design model. Figure 7 depicts the block diagram representation of the closed loop system and defines the inputs and outputs that will be examined to evaluate the performance of candidate controllers.

Regulator Design.– Steady-state regulator gains were determined which minimized a performance index of the form

$$J_R = \lim_{t_1 \to \infty} \frac{1}{t_1} E\left\{\int_0^{t_1} \left(\tilde{x}^T(t)R_1\tilde{x}(t)+u_{FS}^T(t)R_2u_{FS}(t)\right)dt\right\} \tag{7}$$

where E is the expected value operator. R_1 is null and R_2 is the identity. This choice of weighting matrices, plus the constraint that the closed loop system be stable, results in a solution which reflects unstable poles about the imaginary axis, leaving stable poles fixed. This is also the minimum control effort solution which stabilizes the system (Ref. 7). Nevertheless, by reflecting the unstable poles, it provides a finite margin of stability.

Estimator Design.- Steady-state Kalman filter gains were determined which minimize the performance index

$$J_E = \lim_{t_1 \to \infty} \frac{1}{t_1} E\left\{\int_0^{t_1} e^T(t)e(t)dt\right\} \tag{8}$$

for the system defined in (6) where

$$e(t) = \tilde{x}(t) - \hat{x}(t) \tag{9}$$

and $\hat{x}(t)$ satisfies (The reference to t is dropped for compactness.),

$$\dot{\hat{x}} = \tilde{A}\hat{x} + \tilde{B}_u u + L\,[y-\tilde{C}\hat{x}]\ . \tag{10}$$

Here,

$$E\left[\begin{pmatrix}\tilde{B}_w \\ \tilde{D}_w\end{pmatrix} ww^T\begin{pmatrix}\tilde{B}_w^T & \tilde{D}_w^T\end{pmatrix}\right] = \begin{bmatrix}\tilde{B}_uR_u\tilde{B}_u^T+\tilde{B}_gR_g\tilde{B}_g^T & \tilde{B}_gR_g\tilde{D}_g^T \\ \tilde{D}_gR_g\tilde{B}_g^T & \tilde{D}_gR_g\tilde{D}_g^T+R_m\end{bmatrix} = \begin{bmatrix}V_1 & V_{12} \\ V_{12}^T & V_2\end{bmatrix} \tag{11}$$

so that the state excitation and observation noises are correlated. The correlation is a result of the modeling of aerodynamic forces due to gust inputs (Eq. (4)). The coupling term has a minor impact on the resulting control law designs. The solution for the steady-state Kalman filter gain is given by (Ref. 30)

$$L = [PC^T+V_{12}]V_2^{-1} \tag{12}$$

where P, the steady-state covariance of the estimate, satisfies the algebraic Riccatti equation

$$[\tilde{A}-V_{12}V_2^{-1}\tilde{C}]P + P[\tilde{A}-V_{12}V_2^{-1}\tilde{C}]^T + P\tilde{C}^TV_2^{-1}\tilde{C}P + V_1 - V_{12}V_2^{-1}V_{12}^T = 0 \tag{13}$$

The estimator equation may be rewritten as

$$\dot{\hat{x}} = [\tilde{A} - \tilde{B}_u F - L\tilde{C}]\hat{x} + Ly \tag{14}$$

where $u_{FS} = F\hat{x}$ and $-F$ is the solution to equation (7).

Robustness Recovery.– Full state feedback control laws designed using LQ methodology are known to possess good robustness properties (Refs. 31,32). LQG designs, however, may exhibit unsatisfactory robustness characteristics. The introduction of fictitious process noise at the control input has been shown to provide robustness recovery in LQG designs (Ref. 6). Consequently, several estimator designs were performed in which the process noise intensity, R_u, was varied to obtain an acceptable tradeoff between stability margins, control law bandwidth, and available control power. Results for two of the designs are summarized in figures 8 and 9. The loop transfer function Nyquist plots of figure 8 show how the stability margins improve with increasing process noise at the actuator input (the full order evaluation model of the plant was employed in constructing Fig. 8). The Bode plots of figure 9, however, reveal the undesirable feature that the commanded control input at high frequencies becomes larger with increasing input process noise. The controller corresponding to $R_u = (0.79\ \text{deg})^2$ was selected as a basis for initiating the search for a reduced order controller. Note that this controller meets the specified stability margin criteria. Its control requirements, not shown, are also well within the ±15°, ±740°/sec capabilities of the actuator.

Reduced Order Controller Selection

The 25th order controller developed using LQG techniques was reduced to obtain an implementable control law. Figure 10 shows the closed loop block diagram of plant and controller where the controller state space representation is given by

$$\dot{x}_c = A_c x_c + B_c y \tag{15}$$

and

$$u_{FS} = C_c x_c \tag{16}$$

For the case of a full order controller, A_c and B_c are defined by equations (13) and (14) and $C_c = F$.

Order reduction was initiated by transforming (15) to block diagonal form and examining the poles, zeros and residues of the full order (u_{FS}/y) transfer function. Modal truncation was then performed in the transformed domain to obtain the following candidate reduced order controller.

$$\frac{u_{FS}}{y} = \frac{\tilde{F}_o 692.3}{s+692.3} \; \frac{(s+98.59)(s+213.5)}{s^2+118.8s+66.29^2} \; \frac{s^2+214.9s+164.5^2}{s^2+58.48s+94.42^2} \; \frac{s^2+1.030s+136.4^2}{s^2+2.411s+136.9^2} \; \frac{s^2+251.1s+314.1^2}{s^2+406.1s+567.9^2} \tag{17}$$

where $\tilde{F}_o = 0.5064$ deg/g was selected so that the static gain of the full order and reduced order controllers were the same.

The sharp notch at 136 rad/sec essentially cancels the peak in the (y/u) transfer function due to the lowly damped fore and aft wing mode. In some cases, e.g. if the flutter mode frequency were nearly coincident with the notch, failure of the notch to correspond to the frequency of the lowly damped mode might lead to instability. For the case under study, the flutter mode remains separated from the notch at dynamic pressures near the design point. Furthermore, ground vibration tests indicate that the frequency of this mode is actually much higher (220 rad/sec) and that a substantial amount of structural damping is present. Thus, when the design is repeated with the updated structural model, the notch will be widened and occur at a frequency much higher than the frequency of flutter.

Figure 11 presents the Nyquist plot of the system loop transfer function obtained by use of the reduced order controller and the evaluation model of the plant. It is seen, by comparing with figure 8b, that the reduced order controller provides essentially the same stability margins as the full order controller. Figure 12 depicts the frequency response of the reduced order controller which is essentially the same as that of the full order controller shown in figure 9b. Figures 11 and 12 indicate that the order reduction has resulted in little degradation in controller performance.

A high pass filter to remove low frequency signals and additional high frequency attenuation will be incorporated in the actual FS implementation. The impact of phase changes due to such elements will be considered in future design studies.

Scheduling Law for Improved Off Design Performance

The closed loop system is unstable at the evaluation points on the desired flutter boundary (FS -on) with the controller defined in equation (17). Furthermore, $\tilde{F}_o$ is higher than required at dynamic pressures below that of the design point. Performance at off-design points is improved by scheduling the gain as a function of dynamic pressure. The schedule is defined in equation (18).

$$\begin{aligned}
\tilde{F} &= 0.50\ \tilde{F}_o \quad \text{for } q < 400 \text{ lb/ft}^2 \\
\tilde{F} &= [0.50 + 0.00232(q - 400)]\tilde{F}_o \quad \text{for } 400 \leq q \leq 940 \text{ lb/ft}^2 \\
\tilde{F} &= 1.75\ \tilde{F}_o \quad \text{for } q > 940 \text{ lb/ft}^2
\end{aligned} \tag{18}$$

Table 2 shows the performance of the scheduled controller at each of the points indicated in figure 5. The rms control deflection and rate requirements were computed using the frequency domain form (Eq. (2)) of the evaluation model of the plant, the scheduled reduced order controller, and a von Karman input gust spectrum having a 12 fps rms. It was assumed that the measurement noise and fictitious process noise were zero. Good phase and gain margins are achieved near the design point. The system is stable for cases 7 and 8 which are on the desired flutter boundary (FS-on) of figure 5. The control power violations at these two high q cases are not of particular concern since flight tests will not be made at these extreme conditions.

Optimization of the Robustness of Reduced Order Controllers

An alternate design approach will now be employed which allows explicit consideration of design criteria. The approach requires that the form of the control law be specified. Consequently, it is particularly applicable in modifying an existing control law when small changes occur in the plant or in satisfying design criteria not fully considered in the previous design. In the discussion to follow, robustness design criteria will be emphasized.

Constrained minimization techniques (Refs. 10-13) can be employed to determine the benefits of maximizing the minimum singular value of the return difference transfer function subject to explicit constraints on gain margins, phase margins, control power and controller frequency rolloff characteristics. The nonlinear programming algorithm (Refs. 15,16) selected to carry out this optimization requires no gradient computations. Some initial results illustrating the procedure follow.

A reduced order controller of the form of equation (17) was found which maximized the minimum singular value of the return difference transfer function for a flight condition at h = 15,000 feet, $\overline{M} = 0.91$ (See Fig. 5). Nine of the controller coefficients of equation (17) were allowed to vary as indicated in equation (19)

$$u_{FS} = \frac{a_1 (s + a_2)(s + a_3)}{s^2 + a_4 s + a_5} \; \frac{s^2 + a_6 s + a_7}{s^2 + a_8 s + a_9} \, T(s) \tag{19}$$

where

$$T(s) = \frac{692.3}{s + 692.3} \; \frac{s^2 + 1.031s + 136.4^2}{s^2 + 2.411s + 136.9^2} \; \frac{s^2 + 251.1s + 314.1^2}{s^2 + 406.1s + 567.9^2} \tag{20}$$

was fixed. The following constraints were imposed

$$0.25 < a_1 < 2.25$$

$$40 < a_2 < 120$$
$$150 < a_3 < 300$$

$$50 < a_4 < 175$$

$$2000 < a_5 < 5000$$

$$125 < a_6 < 325$$

$$20{,}000 < a_7 < 35{,}000$$

$$30 < a_8 < 90$$

$$6{,}000 < a_9 < 12{,}000$$

$$|\phi_m| > 40°$$

$$|F_m| > 6dB$$

$$N_c = 1$$

$$(\delta a)_{rms} < 15°$$

$$(\dot{\delta} a)_{rms} < 740°/sec$$

The direct constraints upon the design variables were satisfied by making the transformation (Ref. 33)

$$a_i = \frac{1}{2} \left[(a_{u_i} - a_{\ell_i}) \sin \frac{\pi}{2} a_i' + a_{u_i} + a_{\ell_i} \right] \tag{21}$$

Here N_c is the number of counterclockwise encirclements of the -1 point as ω varies from 0 to ∞, ϕ_m is phase margin and F_m is gain margin. The stability of the closed loop system is determined by evaluating N_c. A constrained optimization is carried out as follows:

1. Let c be the vector of inequality constraint functions and define -

   $$\bar{c}_i = \max(0, c_i - c_{u_i}, c_{\ell_i} - c).$$

2. Define a positive definite diagonal weighting matrix W.

3. Form the augmented function

   $$\Phi_W(a') = \frac{1}{2} \frac{1}{\sigma_{min}{}^2} + \frac{1}{2} \bar{c}^T W \bar{c} + 10^{50} |N_c - 1|. \tag{22}$$

4. Find $(a'_W)^*$ which minimizes Φ_W.

5. Increase the magnitude of W and repeat steps 3 and 4.

In the limit as $W \to \infty$, the solution, if it exists, of (22) will maximize the minimum singular value subject to the imposed constraints (Ref. 34). If no solution exists, one would have to change the form of the control law or relax the constraints.

The results obtained in applying this procedure are presented in figure 13 and in table 3 for a finite weighting matrix W. The system is stable. The minimum singular value is increased 26 percent and gain and phase margin constraints are satisfied to within a 2.5 percent tolerance.

CONCLUDING REMARKS

An implementable control law has been designed for suppression of flutter in the symmetric degrees of freedom for a mathematical model of the DAST ARW-2. Stability margin criteria of ±6dB gain margins and ±45° phase margins are exceeded at the design point which is at a dynamic pressure 16.5 percent above the corresponding FS-off flutter value. A gain schedule was defined which provided at least ±6dB gain and ±45° phase margins at off design points examined which had dynamic pressures lower than the design point dynamic pressure. The FS law, with gain scheduling, resulted in a stable system at points examined on the desired (FS-on) flutter boundary having dynamic pressures up to 82 percent above the corresponding open loop flutter values.

Coupling the ISAC program for definition of plant design and evaluation models with the ORACLS LQG methodology provided an effective tool for design of full order controllers. Addition of process noise at the input allowed stability margin criteria to be met. Reduction of the order of the controller from 25th to 9th was achieved with minimal sacrifice in controller performance.

Constrained optimization techniques were successfully applied to maximize the robustness characteristics of the reduced order controller at one flight condition. The nonlinear programming algorithm used required no gradient computations. Stability of the candidate control law at each iteration was determined by computing the number of counterclockwise encirclements of the -1 point made by the open loop transfer function as ω varied from 0 to ∞.

New control laws will be designed for both symmetric and antisymmetric degrees of freedom as the mathematical model of the ARW-2 is improved. At that time, control power and robustness constraints will again be explicitly included in the constrained optimization solution for reduced order controllers.

REFERENCES

1. Peele, Ellwood L.; and Adams, William M., Jr.: A Digital Program for Calculating the Interaction Between Flexible Structures, Unsteady Aerodynamics, and Active Controls. NASA TM 80040, January 1979.

2. Mahesh, J. K.; Stone, C. R.; Garrard, W. L.; and Hausman, P. D.: Active Flutter Control for Flexible Vehicles. NASA CR 159160, November 1979.

3. Roger, Kenneth L.: Airplane Math Modeling Methods for Active Control Design. AGARD CR 228, August 1977.

4. Schwanz, Robert C.: Consistency in Aircraft Structural and Flight Control Analysis. AGARD CR 228, August 1977.

5. Armstrong, Ernest S.: ORACLS - A Design System for Linear Multivariable Control. Marcel Dekker, Inc., c.1980.

6. Doyle, J. C.; and Stein, G.: Robustness with Observers. IEEE Transactions on Automatic Control, August 1979.

7. Kwakernaak, Huibert; and Sivan, Raphael: Linear Optimal Control Systems. Wiley-Interscience, c.1972.

8. Gangsaas, Dagfin; and Ly, Uy-Loi: Application of Modified Linear Quadratic Gaussian Design to Active Control of a Transport Airplane. AIAA Paper No. 79-1746, August 1979.

9. Mukhopadhyay, V.; Newsom, J. R.; and Abel, I.: A Direct Method for Synthesizing Low-Order Optimal Feedback Control Laws with Application to Flutter Suppression. AIAA Paper No. 80-1613, August 1980.

10. Schy, A. A.: Nonlinear Programing in the Design of Control Systems with Specified Handling Qualities. Proceedings of 1972 IEEE Conference on Decision and Control, New Orleans, LA, December 1972.

11. Schy, A. A.; Adams, William M., Jr.; and Johnson, K. G.: Computer-Aided Design of Control Systems to Meet Many Requirements. NATO AGARD Conference Proceedings No. 137 on Advances in Control Systems, 1973.

12. Knox, J. R.; and McCarty, J. M.: Algorithms for Computation of Optimal Constrained Output Feedback for Linear Multivariable Systems. AIAA Paper No. 78-1290, August 1978.

13. Adams, William M., Jr.: and Tiffany, Sherwood H.: Control Law Design to Meet Constraints Using SYNPAC--Synthesis Package for Active Controls. NASA TM 83264, January 1982.

14. Newsom, Jerry R.; and Mukhopadhyay, V.: The Use of Singular Value Gradients and Optimization Techniques to Design Robust Controllers for Multiloop Systems. AIAA Paper No. 83-2191, August 1983.

15. Olsson, D. M.: A Sequential Simplex Program for Solving Minimization Problems. Journal of Quality Technology, Vol. 6, No. 1, January 1974, pp. 53-57.

16. Olsson, Donald M.; and Nelson, Lloyd S.: The Nelder-Mead Simplex Procedure for Function Minimization. Technometrics, Vol. 17, No. 1, February 1975.

17. Sliwa, Steven M.: Use of Constrained Optimization in the Conceptual Design of a Medium-Range Subsonic Transport. NASA TP 1762, December 1980.

18. Arbuckle, P. Douglas; and Sliwa, Steven M.: Parametric Study of Critical Constraints for a Canard Configured Medium Range Transport Using Conceptual Design Optimization. AIAA Paper No. 83-2141, August 1983.

19. Boeing Wichita Company: Integrated Design of a High Aspect Ratio Research Wing with an Active Control System for Flight Tests on a BQM-34E/F Drone Vehicle. NASA CR 166108, 1979.

20. Boeing Wichita Company: Integrated Design of a High Aspect Ratio Research Wing with an Active Control System for Flight Tests on a BQM-34E/F Drone Vehicle. NASA CR 166109, 1979.

21. Albano, E.; and Rodden, W. P.: A Doublet Lattice Method for Calculating Lift Distributions on Oscillating Surfaces in Subsonic Flows. AIAA Journal, Vol. 7, No. 2, February 1969, pp. 279-285.

22. Giesing, J. P.; Kalman, T. P.; and Rodden, W. P.: Subsonic Unsteady Aerodynamics for General Configurations. AFFDL-TR-71-5, November 1971.

23. Jones, R. T.: The Unsteady Lift of a Wing of Finite Aspect Ratio. NACA Rept. 641, 1940.

24. Vepa, R.: Finite State Modeling of Aeroelastic Systems. Ph.D. Dissertation, Department of Applied Mechanics, Stanford University, June 1975.

25. Edwards, John W.: Unsteady Aerodynamic Modeling and Active Aeroelastic Control. SUDAAR 504, February 1977.

26. Dunn, H. J.: An Analytical Technique for Approximating Unsteady Aerodynamics in the Time Domain. NASA TP 1738, November 1980.

27. Boeing Commercial Aircraft Company Staff: Integrated Application of Active Controls (IAAC) Technology to an Advanced Subsonic Transport Project - Wing Planform Study and Final Configuration Selection. NASA CR 165630, June 1981.

28. Military Specifications - Flying Qualities of Piloted Airplanes. MIL-F-8785C, November 5, 1980. (Superseding MIL-F-8785B, August 7, 1969.)

29. Newsom, J. R.; Pototsky, Anthony S.; and Abel, I.: Design of the Flutter Suppression System for DAST ARW-1-1R - A Status Report. NASA TM 84642, March 1983.

30. Wonham, W. M.: Stochastic Problems In Optimal Control. 1963 IEEE Convention Record, Part 2, 1963, pp. 114-124.

31. Kalman, R. E.: When is a Linear System Optimal? Trans. ASME Ser. D.: Journal of Basic Engineering, Vol. 86, March 1964, pp. 51-60.

32. Safonov, M. G.; and Athans, M.: Gain and Phase Margins for Multiloop LQG Regulators. IEEE Transactions on Automatic Control. Vol. AC-22, April 1977, pp. 173-179.

33. Park, Steven K.: A Transformation Method for Constrained-Function Minimization. NASA TN D-7983, November 1975.

34. Courant, R.: Variational Methods for the Solution of Problems of Equilibrium and Vibrations. Bull. American Math Society, Vol. 49, January 1943, pp. 1-23.

Table 1. Natural Frequencies of Free-Free Symmetric Elastic Modes

elastic mode number	frequency, hz
1	7.847
2	14.21
3	21.72
4	30.27
5	33.28
6	41.10
7	47.01
8	63.06
9	67.22
10	78.24

Table 2.- Performance of scheduled, reduced-order controller.

case number	q lb/ft^2	h feet	M	$(\delta a)_{rms}$ deg	$(\dot{\delta} a)_{rms}$ deg/sec	Gain Margin at ω dB rad/sec	Phase margin at ω deg rad/sec
1	547	18,000	0.86	4.08	449	-16.9 at 116 13.5 at 441	-72.5 at 95.6 68.1 at 159
2	576	15,000	0.83	4.03	465	-13.9 at 121 12.0 at 444	-74.4 at 88.2 52.5 at 165
3	614	13,400	0.83	4.44	523	-8.92 at 125 10.6 at 444	-66.5 at 88.0 43.3 at 166
4	619	15,000	0.86	4.94	563	-7.31 at 122 10.8 at 441	-53.8 at 96 45.2 at 162
5	670	13,000	0.86	5.41	629	-5.54 at 127 9.15 at 442	-47.3 at 94.5 35.6 at 165
6	692	15,000	0.91	5.76	599	-6.08 at 122 7.33 at 437	-28.2 at 86.8 41.8 at 174
7	912	8,000	0.91	14.2	1143	-4.26 at 136 2.13 at 68.7	-3.25 at 74.7 32.9 at 203
8	938	4,250	0.86	7.90	837	-3.43 at 150 3.47 at 445	-14.2 at 75.6 22.9 at 190

Table 3.- Comparison of controller optimized for robustness with nominal controller (h=15,000 feet, M=0.91)

Function, Constraint, and Design Variables	Optimized Controller	Nominal Controller
singular value	0.587 at 434 rad/sec	0.465 at 93.4 rad/sec
$(\delta a)_{rms}$, deg	5.23	5.68
$(\dot{\delta} a)_{rms}$, deg/sec	561	612
gain margin, dB	-5.92 at 123 rad/sec 7.69 at 433 rad/sec	-4.64 at 122 rad/sec 8.77 at 437 rad/sec
phase margin, deg	-38.8 at 91.2 rad/sec 39.0 at 177 rad/sec	-27.1 at 94.6 rad/sec 40.5 at 164 rad/sec
a_1, deg/g	0.543	0.506
a_2, sec^{-1}	106	98.6
a_3, sec^{-1}	234	213
a_4, sec^{-1}	116	119
a_5, sec^{-2}	4529	4395
a_6, sec^{-1}	242	215
a_7, sec^{-2}	26429	27076
a_8, sec^{-1}	65.1	58.5
a_9, sec^{-2}	7887	8915

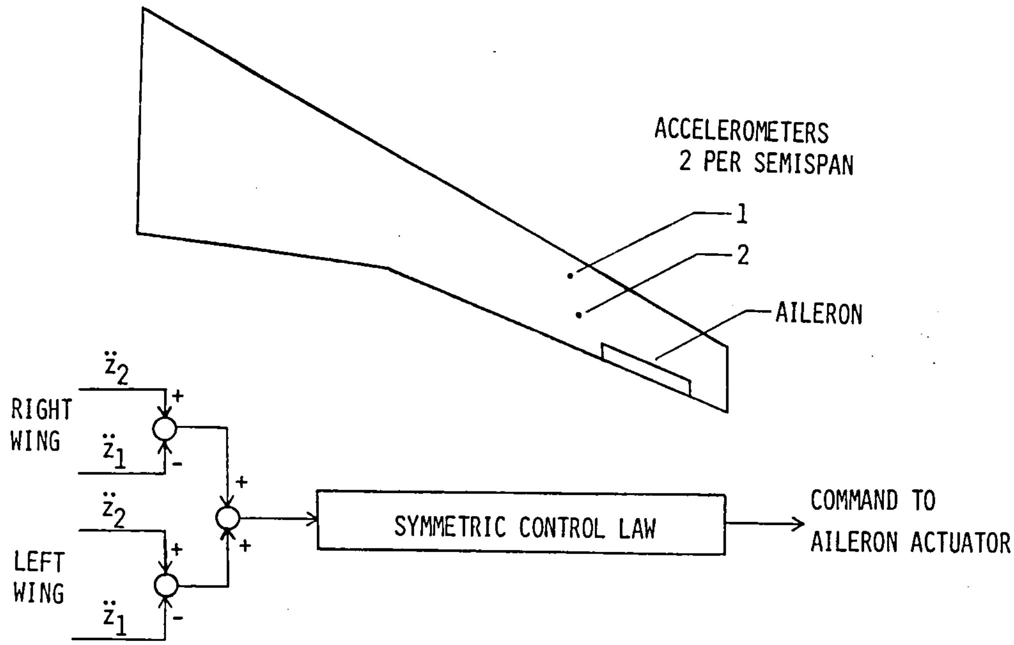

Figure 1.- Sensor signal inputs to symmetric flutter suppression control law.

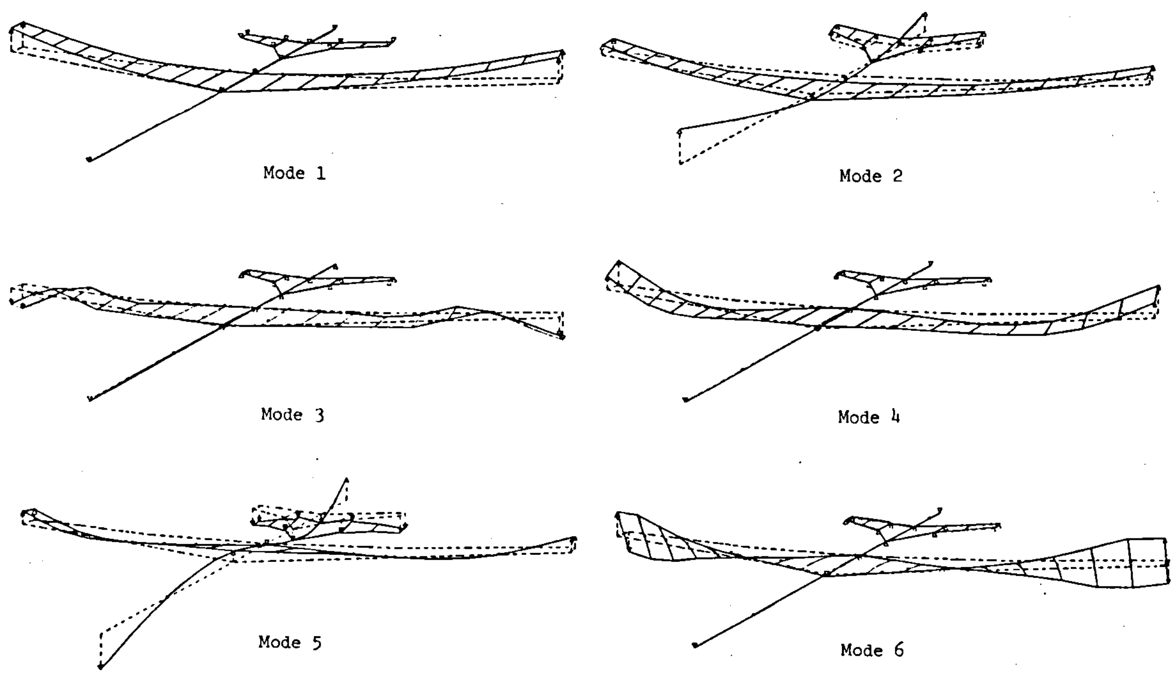

Figure 2. Normal components of six lowest frequency symmetric free-free mode shapes

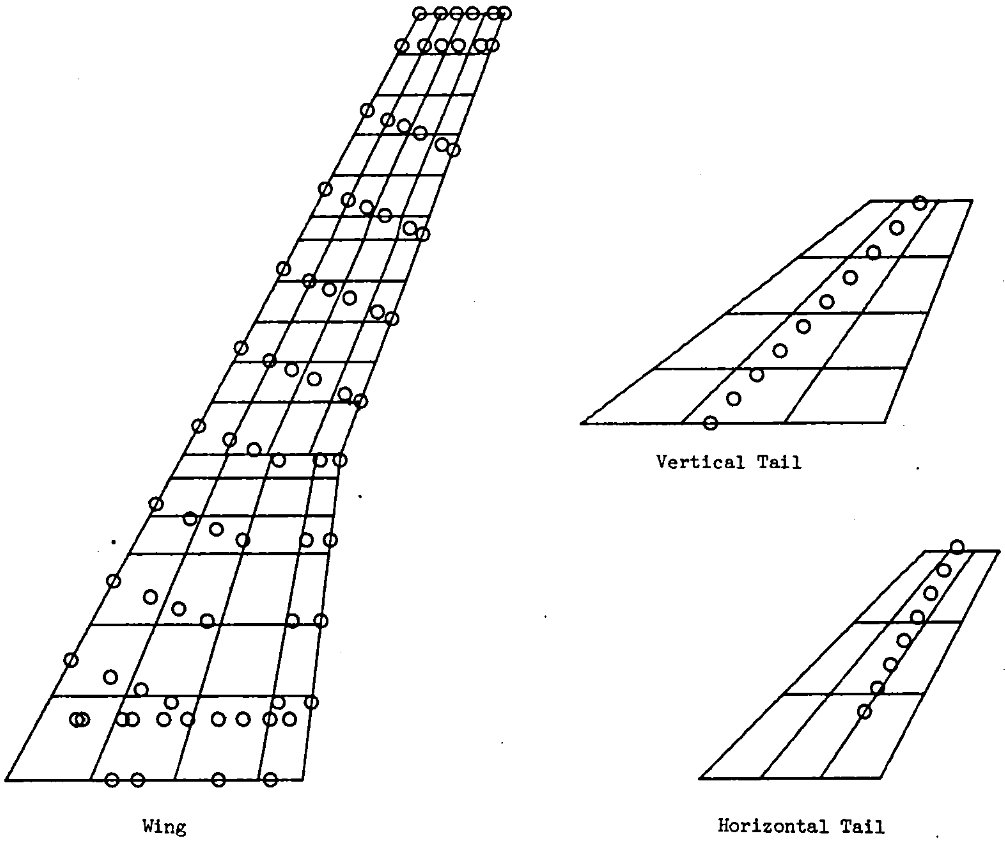

Figure 3. Paneling of lifting surfaces for unsteady aerodynamic force computations

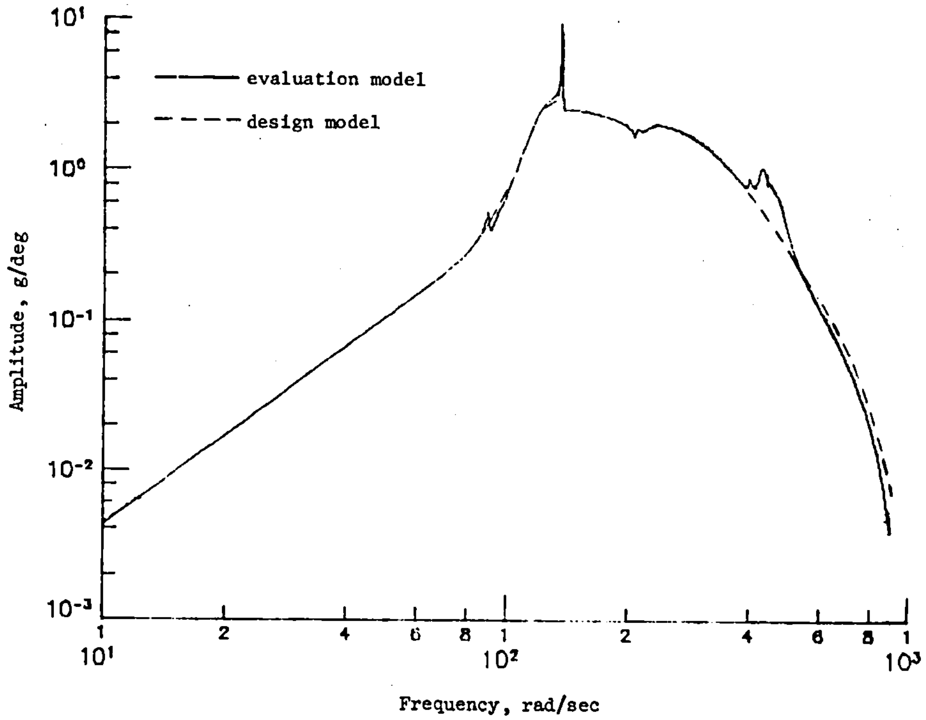

Figure 4.- Amplitude of symmetric component of y/u_R, FS-off ($\bar{M}$ = 0.86, h = 15000 ft).

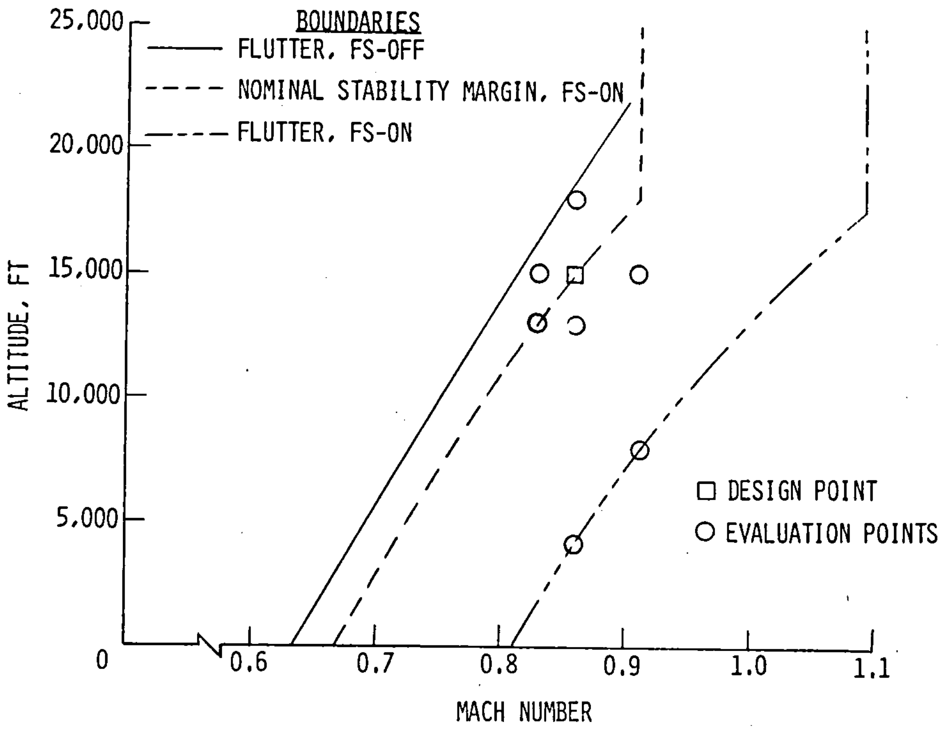

Figure 5.- Flutter boundary, FS-off; nominal stability margin boundary and flutter boundary, FS-on.

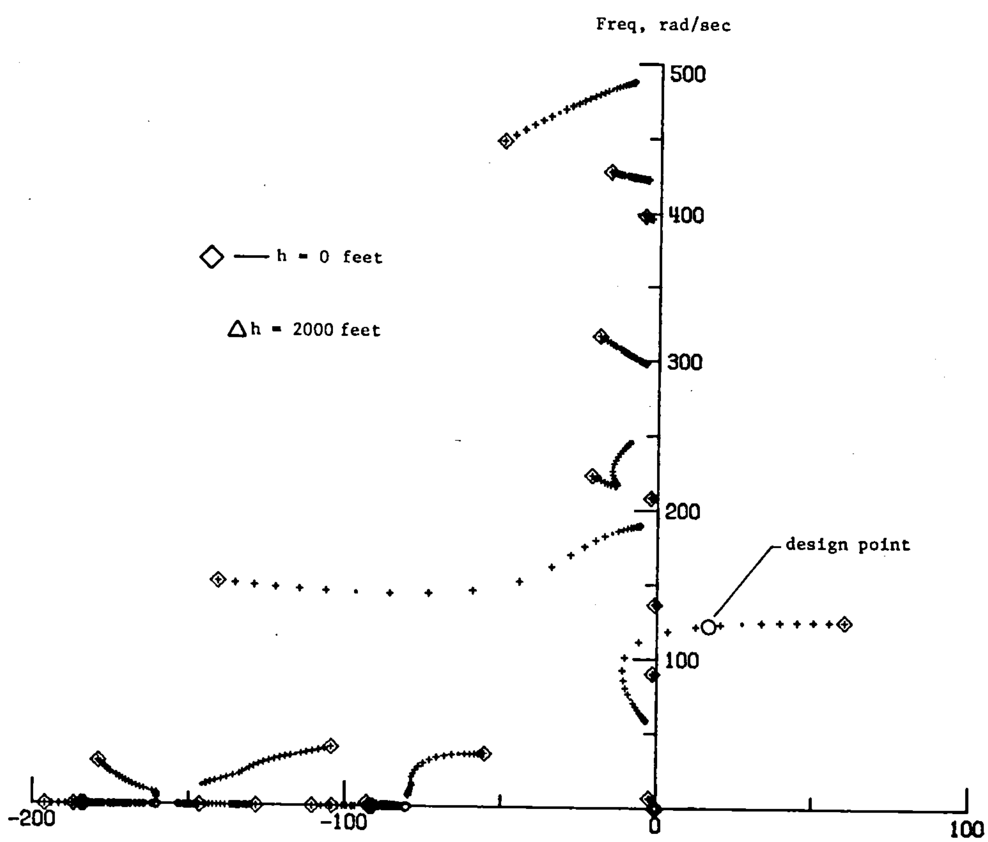

Figure 6.- Variation of symmetric characteristic roots with altitude for a Mach number of 0.86 (evaluation model).

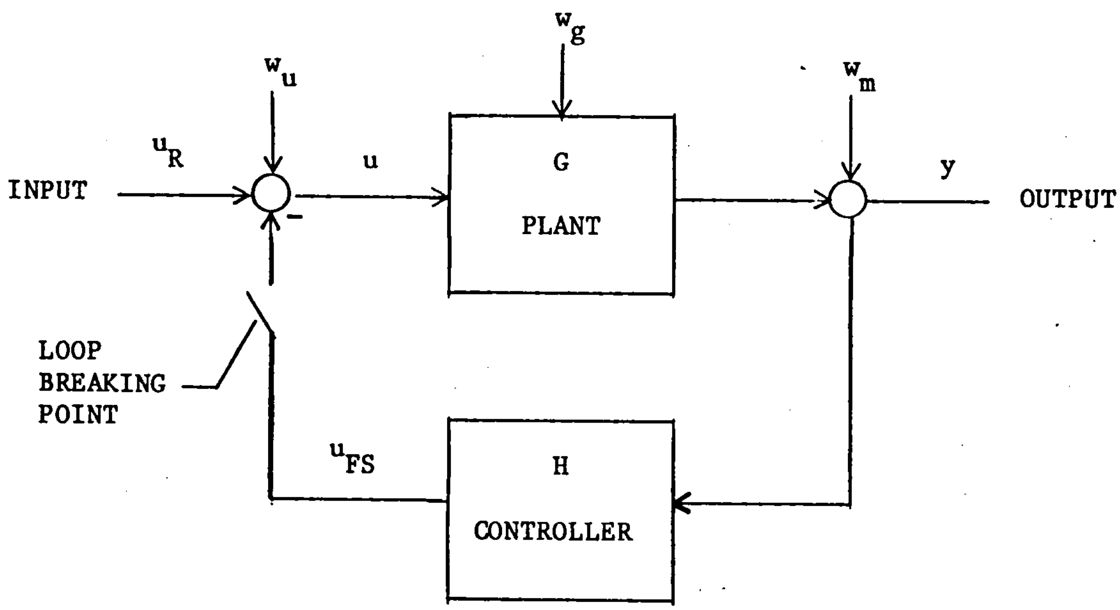

Figure 7.- Closed loop block diagram.

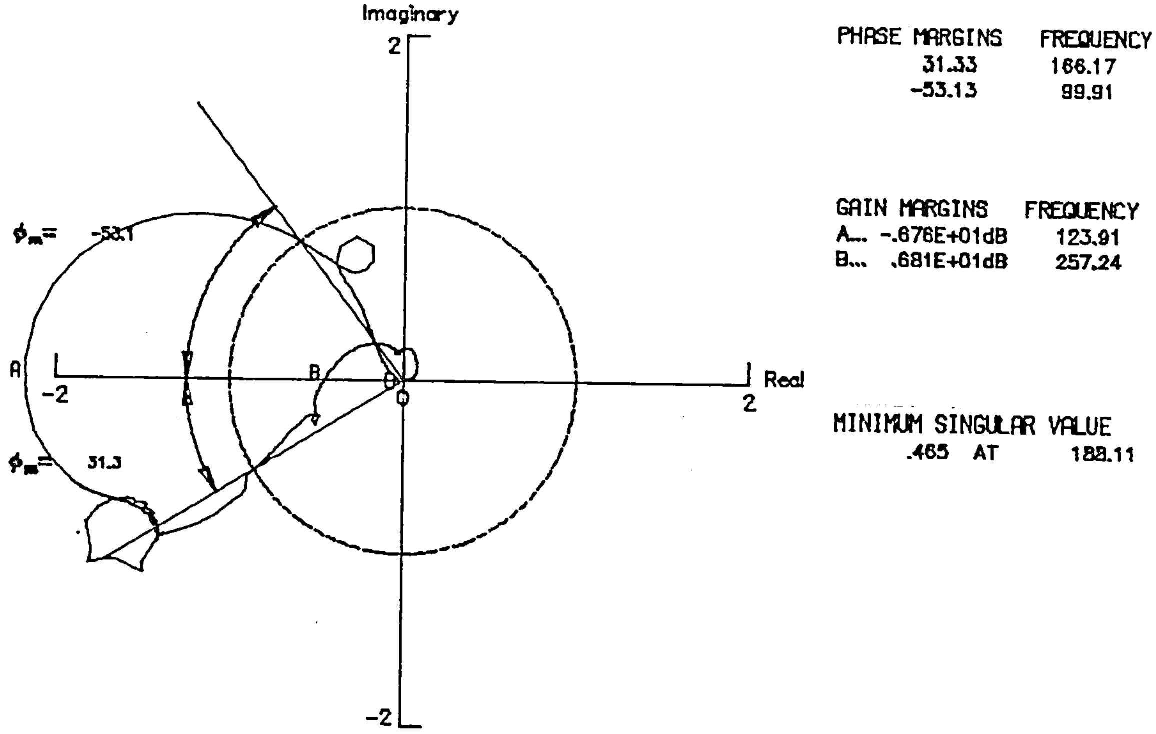

a) $R_u = 0.$

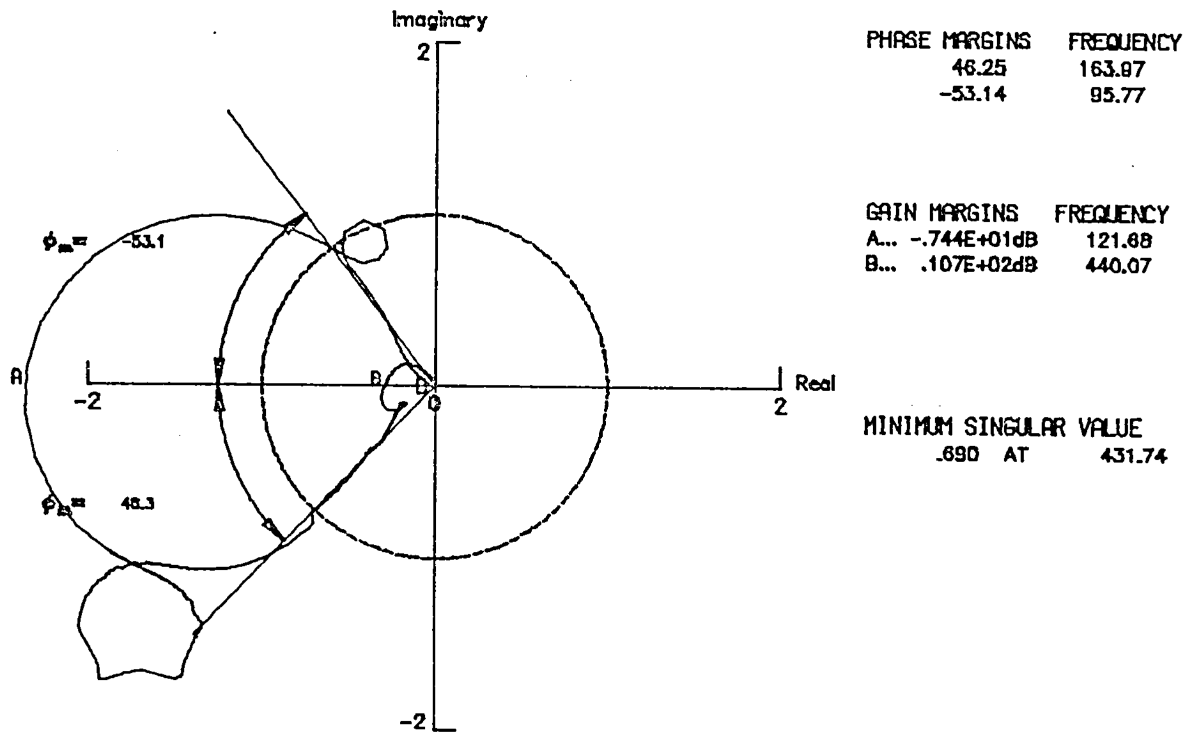

b) $R_u = 0.79^2 \deg^2.$

Figure 8.- Nyquist plots of HG transfer function at the design point using full order controller.

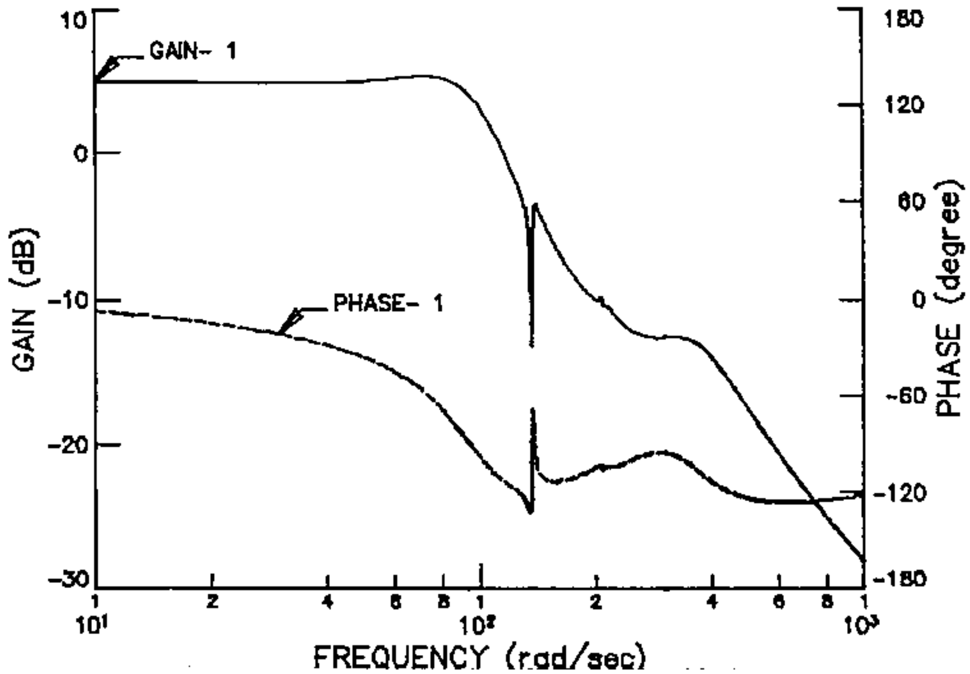

a) $R_u = 0.$

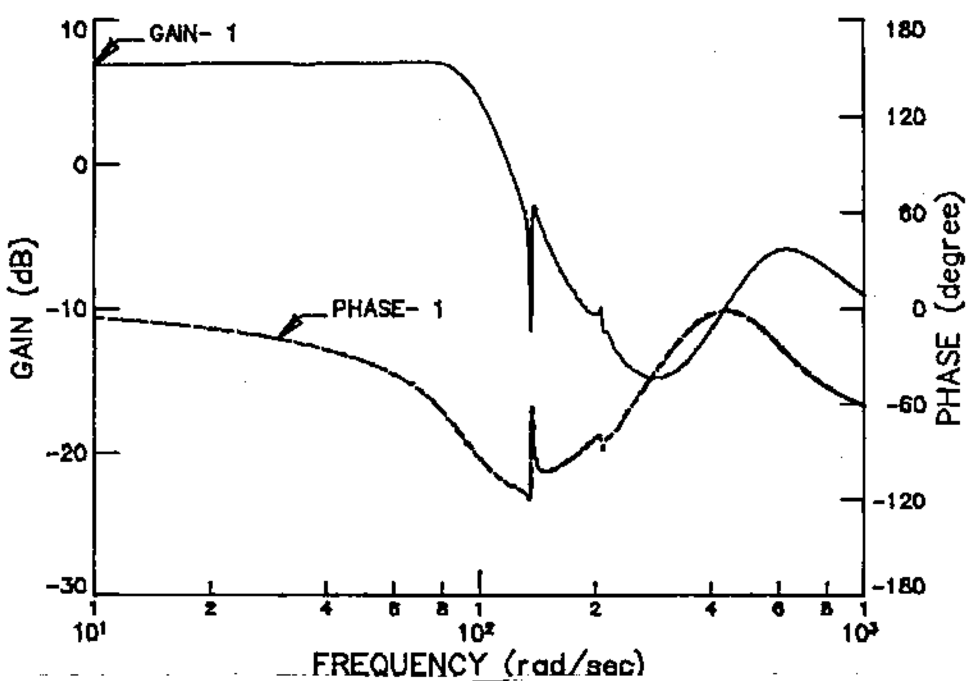

b) $R_u = 0.79^2 \deg^2.$

Figure 9.- Bode plots of full order controller, u_{FS}/y.

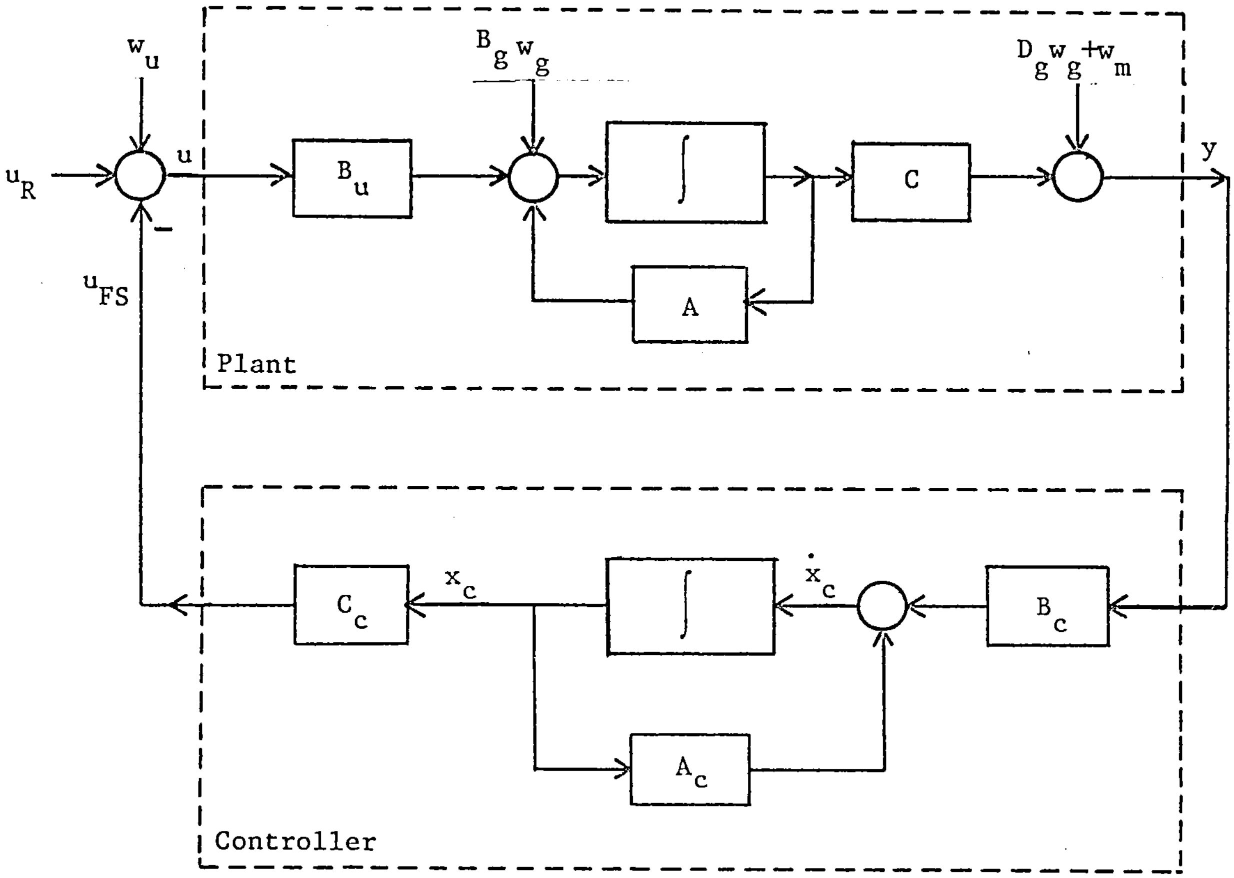

Figure 10.- Closed loop system.

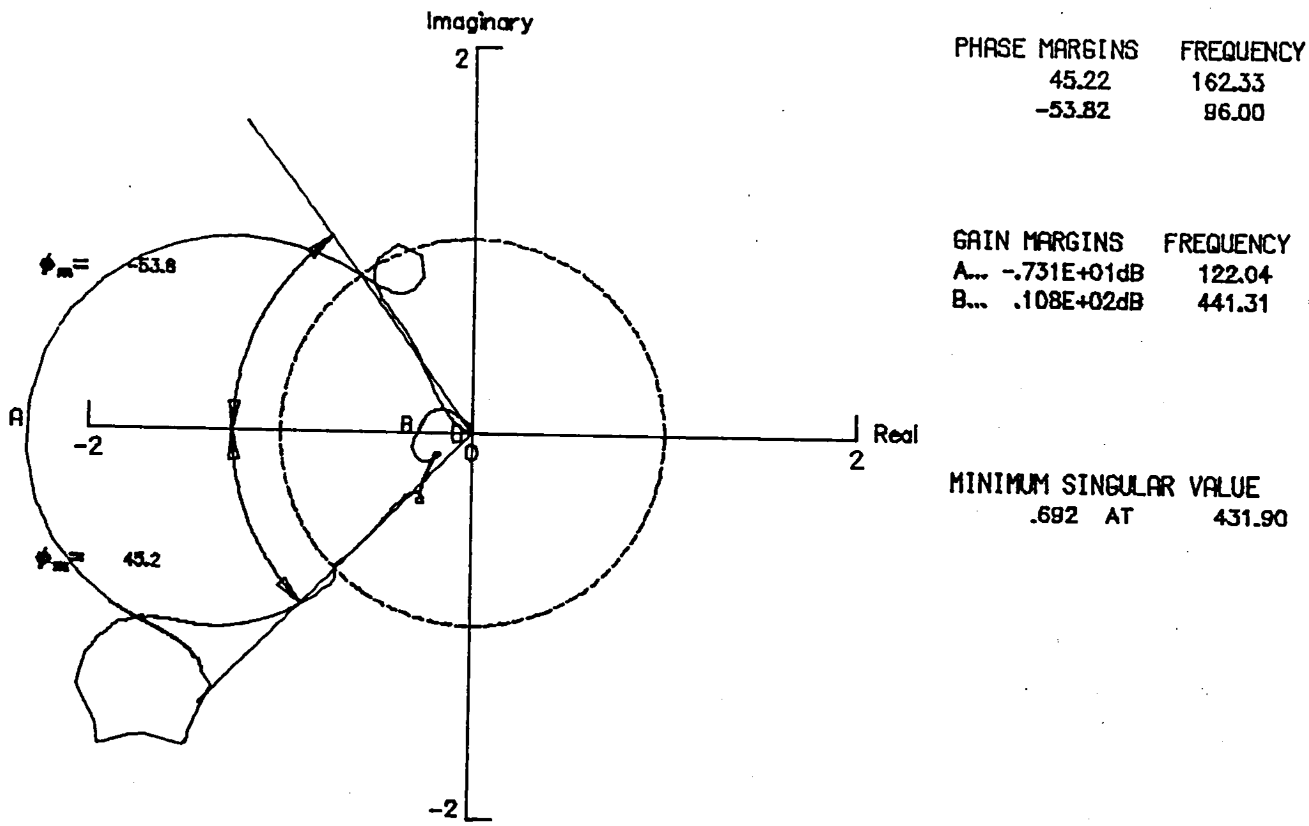

Figure 11.- Nyquist plot of HG transfer function for reduced order controller at the design point.

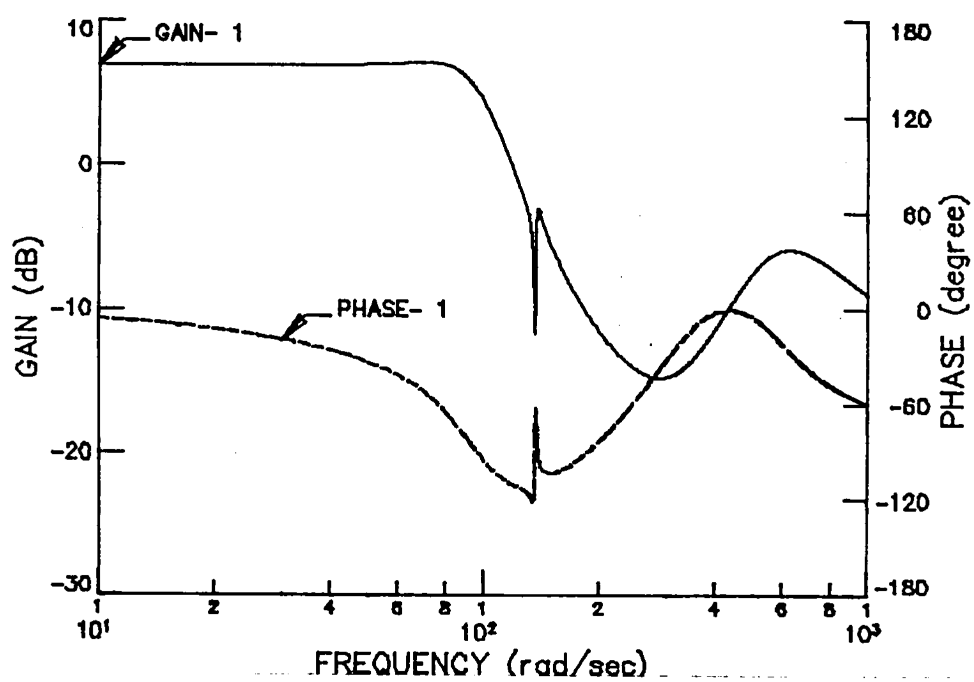

Figure 12.- Bode plot of reduced order controller transfer function (H), deg/g, at the design point.

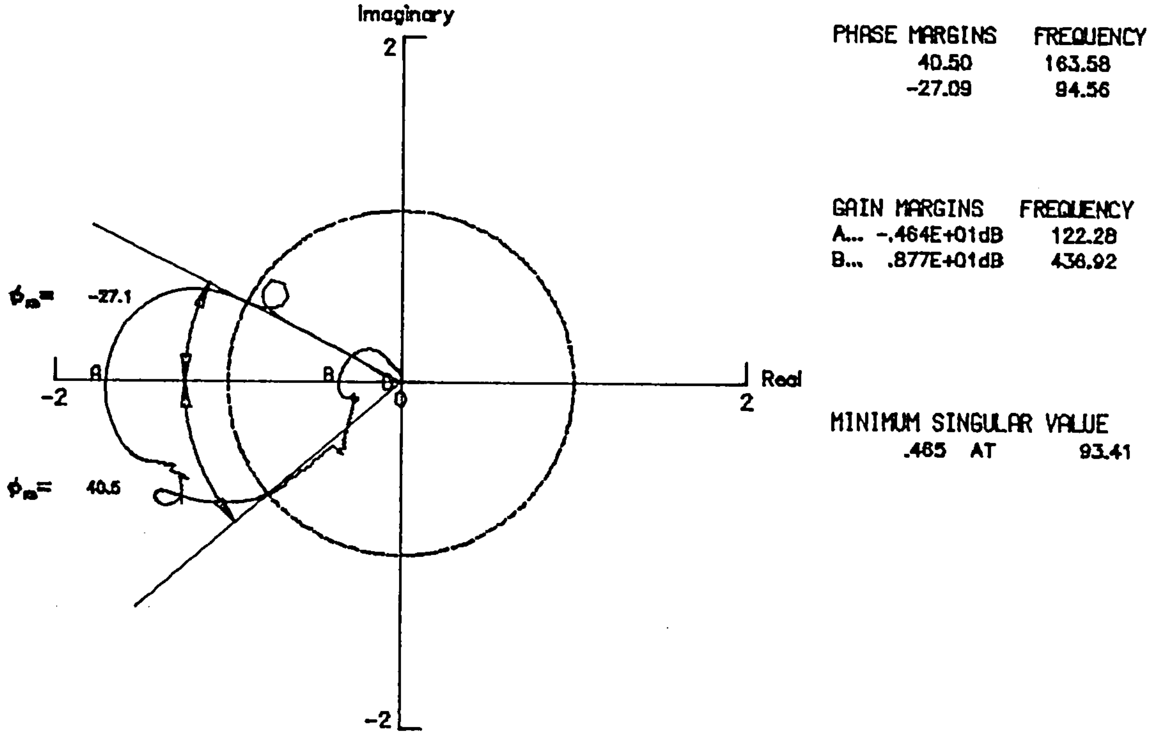

a) nominal, reduced order controller.

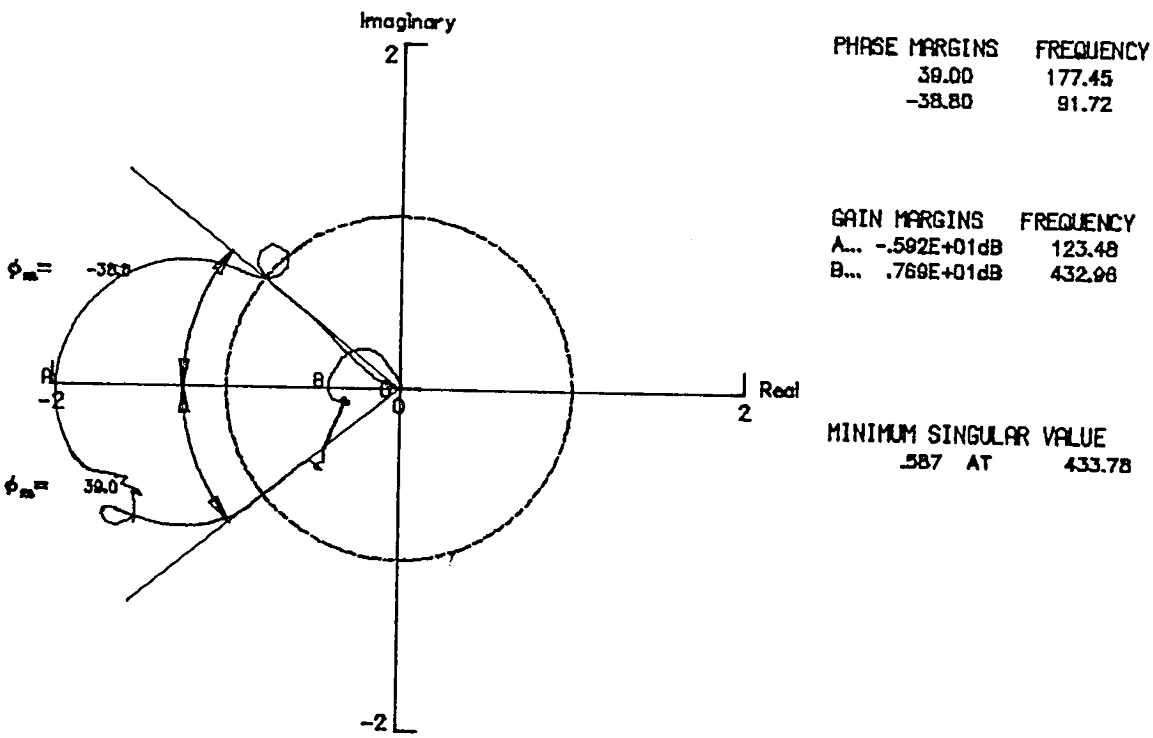

b) optimized reduced order controller.

Figure 13.- Nyquist plot of HG transfer function
(M = 0.91, h = 15000 ft).

1. Report No. NASA TM-86257	2. Government Accession No.	3. Recipient's Catalog No.
4. Title and Subtitle Design of a Candidate Flutter Suppression Control Law for DAST ARW-2		5. Report Date July 1984
		6. Performing Organization Code 505-34-03-05
7. Author(s) William M. Adams, Jr. and Sherwood H. Tiffany		8. Performing Organization Report No.
9. Performing Organization Name and Address NASA Langley Research Center Hampton, VA 23665		10. Work Unit No.
		11. Contract or Grant No.
12. Sponsoring Agency Name and Address National Aeronautics and Space Administration Washington, DC 20546		13. Type of Report and Period Covered Technical Memorandum
		14. Sponsoring Agency Code

15. Supplementary Notes

This paper is the written version of AIAA Paper No. 83-2221 entitled, "Design of a Candidate Flutter Suppression Control Law for DAST ARW-2," which was presented at the 1983 AIAA Guidance and Control Conference, Gatlinburg, TN, August 15-17, 1983.

16. Abstract

A control law is developed to suppress symmetric flutter for a mathematical model of an aeroelastic research vehicle. An implementable control law is attained by including modified LQG (Linear Quadratic Gaussian) design techniques, controller order reduction, and gain scheduling. An alternate (complementary) design approach is illustrated for one flight condition wherein nongradient-based constrained optimization techniques are applied to maximize controller robustness.

17. Key Words (Suggested by Author(s)) active controls modified LQG reduced-order controllers constrained optimization	18. Distribution Statement Unclassified - Unlimited Subject Category 08

19. Security Classif. (of this report) Unclassified	20. Security Classif. (of this page) Unclassified	21. No. of Pages 27	22. Price A03

DO NOT REMOVE SLIP FROM MATERIAL

Delete your name from this slip when returning material to the library.

NAME	DATE	MS
~~Robert Bartels~~	~~1/99~~	~~340~~